Nanoscale

Accepted Manuscript

This article can be cited before page numbers have been issued, to do this please use: R. Zhou, P. Wang, Y. Guo, X. Dai, S. Xiao, Z. Fang, R. Speight, E. W. W. Thompson, P. Cullen and K. Ostrikov, *Nanoscale*, 2019, DOI: 10.1039/C9NR04951G.

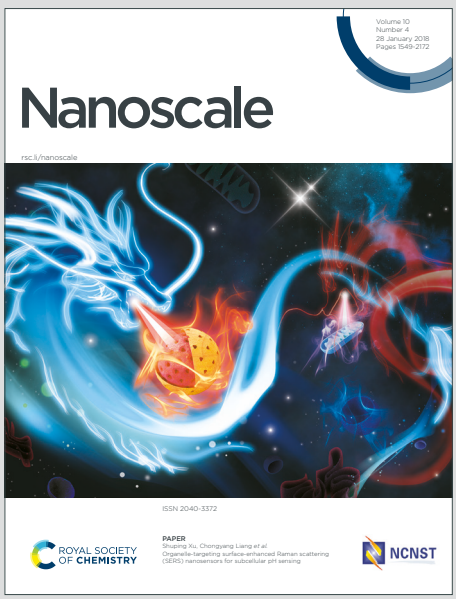

ROYAL SOCIETY OF CHEMISTRY

rsc.li/nanoscale

ROYAL SOCIETY OF CHEMISTRY View Article Online
DOI: 10.1039/C9NR04951G

Journal Name

ARTICLE

Prussian Blue Analogue Nanoenzymes Mitigate Oxidative Stress and Boost Bio-Fermentation

Received 00th January 20xx,
Accepted 00th January 20xx

DOI: 10.1039/x0xx00000x

www.rsc.org/

Renwu Zhou,[#,*,a,b,c] Peiyu Wang,[#,a,b] Yanru Guo,[#,d] Xiaofeng Dai,[e] Shaoqing Xiao,[f] Zhi Fang,[*,g] Robert Speight,[a] Erik W. Thompson,[a,b] Patrick J. Cullen[c] and Kostya (Ken) Ostrikov[a,b]

Oxidative stress in cells caused by the accumulation of reactive oxygen species (ROS) is a common cause of cell function degeneration, cell death and various diseases. Efficient, robust and inexpensive nanoparticles (nanoenzymes) capable of scavenging/detoxifying ROS even in harsh environments are attracting strong interest. Prussian blue analogues (PBAs), a prominent group of metalorganic nanoparticles (NPs) with the same cyanometalate structure as the traditional and commonly used Prussian blue (PB), has long been envisaged to mimic enzyme activities for ROS scavenging. However, their biological toxicity, especially potential effects on living beings during practical application, have not yet been fully investigated. Here we reveal the enzyme-like activity of the FeCo-PBA NPs, and for the first time investigate the effects of the FeCo-PBA on the cell viability and growth. We elucidate the nanoenzyme effect on the ethanol-production efficacy of a typical model organism, the engineered industrial strain *Saccharomyces cerevisiae*. We further demonstarte that the FeCo-PBA NPs have almost no cytotoxicity on the cells over a broad dosage range (0-100 μg/mL), while clearly boosting the yeast fermentation efficiency by mitigationg oxidative stress. The atmospheric pressure cold plasma (APCP) pretreatment is used as a multifunctional environmental stress produced by the plasma reactive species. While the plasma enhances the NP cellular uptake, the FeCo-PBA NPs protect the cells from the oxidative stress induced by both the plasma and the fermentation processes. This synegistic effect leads to the higher secondary metabolite yields and energy production. Collectively, this study confirms the positive effects of PBA nanoparticles in living cells through ROS scavenging, thus potentially opening new ways to control cellular machinery in the future nano-biotechnlogy and nano-biomedical applications.

Introduction

Reactive oxygen species (ROS), derived from metabolic processes in living organisms, are important intermediates for cellular signalling processes and intracellular functions.[1-3] Overproduction and/or dysregulation of ROS, especially the highly reactive ones such as hydrogen peroxide (H_2O_2) and superoxide radicals ($\cdot O_2^-$), will cause oxidative stress in biological systems, directly contributing damages to cellular biomolecules and linked to the occurrence of various diseases and the degeneration or loss of cell functions.[4-6] Methods and agents capable of scavenging ROS and maintaining the balance between the ROS generation and removal have high therapeutic and economic values.[6-8]

Natural antioxidant enzymes in cells such as superoxide dismutase (SOD) and catalase establish protective barriers for cells by detoxifying ROS and reducing damage from oxidative stress.[9-11] However, the applications of the natural enzymes are much impeded from obtaining the desirable activities by their inherent unwelcome properties, such as lack of stability and specific requirements (pH, temperature and even net inhibitors existence), in addition to high cost and issues in large-scale production.[12-14] Recent decades have witnessed fast development of the emerging artificial enzymes, especially based on inorganic nanomaterials (also called nanoenzymes). The nanoenzymes include noble metals, metal oxides, carbon materials featuring not only natural enzyme-like activities but also advantages such as excellent stability and ease-of-synthesis.[15-19]

Prussian blue (PB, $KFe^{III}[Fe^{II}(CN)_6]$) is a well-known and easily-available nanomaterial widely used in magnetics, photo- and electrochemistry, and biomedicine.[20-22] Evidence suggests

[a] Institute of Health and Biomedical Innovation, School of Chemistry, Physics and Mechanical Engineering, Science and Engineering Faculty, Queensland University of Technology, Brisbane QLD 4000, Australia. Email: zhourenwu2015@163.com;
[b] Translational Research Institute, Brisbane, QLD 4102, Australia
[c] School of Chemical and Biomolecular Engineering, The University of Sydney, NSW 2006, Australia
[d] Beijing National Laboratory for Molecular Sciences (BNLMS), College of Chemistry and Molecular Engineering, Peking University, Beijing 100871, China
[e] Wuxi School of Medicine, Jiangnan University, 214122, China
[f] Engineering Research Center of IoT Technology Applications (Ministry of CEducation), Department of Electronic Engineering, Jiangnan University, Wuxi 214122, China.
[g] College of Electrical Engineering and Control Science, Nanjing Tech University, Nanjing 210009, China. Email: myfz@263.net
[#] Equal contribution
†Electronic Supplementary Information (ESI): DOI: 10.1039/x0xx00000x

View Article Online
DOI: 10.1039/C9NR04951G

that PB has inconspicuous toxicity towards a variety of cell types and can harmlessly pass through the body due to its high binding affinity for cyanide ions.[23] Shokouhimehr *et al.* reported that the PB was biocompatible for cellular imaging and drug delivery with high stability and insignificant intracellular production of ROS.[24] Zhang *et al.* also discovered that PB nanoparticles (PB NPs) could effectively scavenge reactive oxygen species (ROS). The ROS scavenging effect of PB NPs is attributed to their affinity for hydroxyl radicals (•OH) and the ability to mimic three antioxidant enzymes including peroxidase (POD), catalase (CAT), and superoxide dismutase (SOD).[23] Meanwhile, the cyanometalate structural analogues of PB (usually termed PB analogue nanoparticles, PBA NPs, $A_xM'[M''(CN)_6]_y{\cdot}nH_2O$, A: alkaline metal; M: transition metal; $0 \leq x \leq 2$; $y \leq 1$), have attracted strong attention through the many encouraging results in electrocatalysis, molecular magnetism, hydrogen storage, solid cells, and other areas.[25] Recently, PBA NPs effectively mimicked the functions of ROS-scavenging enzymes, thus showing a promise in biotechnology applications.[26] However, the biological effects of PBA NPs, especially their cytotoxicity and ROS scavenging ability, remain largely unexplored.

To fill the gap, in this study, a typical PB analogue, FeCo-PBA, is synthesized and its enzyme-like activities are examined both extracellularly and intracellularly (Fig. S1, ESI†). The FeCo-PBA particles are then used in a yeast fermentation process for enhancing ethanol production and gaining new insights for potential real-world applications. *Saccharomyces cerevisiae* is a widely-used and well-studied unicellular eukaryote facilitating beverage fermentation. Recent findings suggest that in the ethanol fuel production, the viability and fermentative ability of the yeast are both negated by ROS generation during the fermentation. The problem escalates when the produced ethanol accumulates and other stress factors such as pH, temperature, osmotic pressure and fermentation inhibitors, come into play.[27,28] Substantial efforts, especially those based on complex and costly genetic engineering, have been carried out to improve ethanol and ROS tolerance and enhance metabolic activity of *S. cerevisiae* to maximize the benefits in bio-fermentation.[29,30] Here, unique physicochemical atmospheric pressure cold plasma (APCP),[31,32] are applied to stress the yeast cells and validate the anti-oxidative effects of the PBA in a simulated ROS-containing environment (Fig. S2, ESI†).

Results and discussion

Characterization of the synthesized FeCo-PBA NPs

The XRD patterns in the 2 θ range from 10° to 80° of FeCo-PBA nanoparticles is presented in Fig. 1(a). All the main characteristic diffraction peaks could be indexed to FeCo-PBA (JCPDS card No. 89-3736), which is in good agreement with the result of simulated XRD of face-centred cubic (fcc) phase of $Fe_3[Co(CN)_6]_2{\cdot}nH_2O$. The IR spectroscopy present the bonding information of FeCo-PBA nanoparticles. Characteristic peaks located at 2175 cm^{-1} is identified to the C≡N triple bond

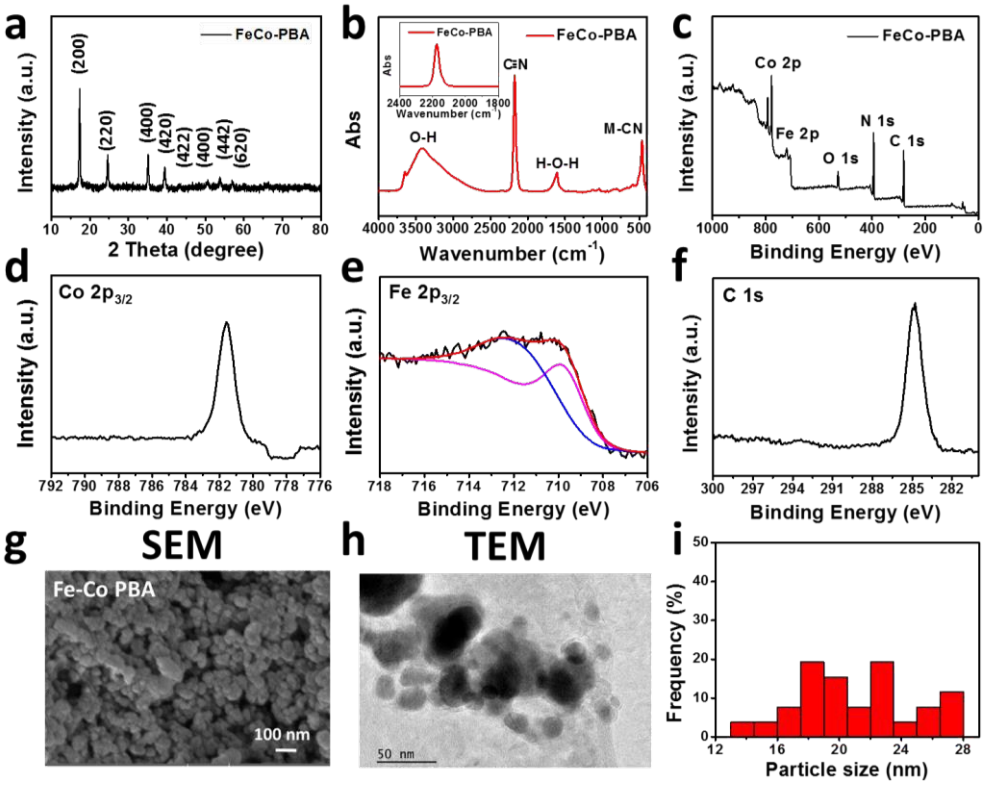

Fig. 1 Characterization of the FeCo-PBA NPs. (a) XRD pattern of FeCo-PBA NPs. (b) FTIR spectra of FeCo-PBA NPs. (c) XPS spectra of FeCo-PBA NPs. (d) Co $2p_{3/2}$ XPS spectra. (e) Fe $2p_{3/2}$ XPS spectra. (f) C 1s XPS spectra. (g) SEM image of FeCo-PBA NPs. (h) TEM image of FeCo-PBA NPs. (i) DLS analysis of the nanoparticles.

stretching mode including vibrations of Fe(III)–CN–Co(II) and Fe(II)–CN–Co(III) due to electron-transfer processes.[33] X-ray photoelectron spectroscopy (XPS) is employed to investigate the valence state of FeCo nanoparticles. Fig. 1(c) shows the overall XPS survey spectrum of the sample. Five elements including carbon, oxygen nitrogen, cobalt and iron are identified. The XPS of Co 2p and Fe 2p contain two doublets of 1/2 and 3/2. Two peaks of Co $2p_{3/2}$ with the binding energies located at 781.5 eV are corresponded to the existence of $[Co(CN)_6]^{3-}$. Similarly, for Fe $2p_{3/2}$, two characteristic peaks at 711.8 eV and 710.1 eV could be assigned to Fe (III) and Fe (II).[34] Fig. 1(g)-(i) shows the morphology structure of FeCo-PBA nanoparticles. Scanning electron microscope (SEM) image (Fig. 1(g)) reveals that the FeCo PBA samples are composed of numerous crystalline nanoparticles with a sphere-like morphology. The transmission electron microscopy (TEM) image (Fig. 1(h)) and the corresponding size distribution histograms show that the diameter of the spherical product is approximately 10–30 nm. The stability of FeCo-PBA NPs is evaluated using UV-vis absorption spectra. Results shows that the optical density at 600 nm (OD_{600}) of the nanoparticle suspension does not decrease with time in aqueous solution (Fig. S3, ESI†), indicating that there is no sedimentation or obvious agglomeration of particles.

Catalase and SOD mimicking activity of FeCo-PBA NPs

H_2O_2 and $\cdot O_2^-$ are two ROS representatives widely produced by different cellular metabolic processes, and both are highly destructive once their amount exceeds the antioxidant capacity of cell themselves.[15] To understand the anti-ROS ability of FeCo-PBA NPs, solutions containing H_2O_2 or $\cdot O_2^-$ are prepared and then combined with NPs, as well as natural enzymes or commercial antioxidants for comparison. The ROS scavenging is quantified by using fluorescent probes. In the presence of FeCo-PBA NPs, the fluorescent intensities significantly decrease just as the Trolox/Tempol and the natural catalase/SOD behave, illustrating that H_2O_2 and $\cdot O_2^-$ can be effectively eliminated, and directly proving that FeCo-PBA NPs possess both catalase- and SOD-like activity. Specifically, more than 75% of H_2O_2 can be eliminated by using 20 μg/mL of pristine FeCo-PBA NPs (without heat pretreatment), the scavenging activity of which is considerably better than those of 100 μM of synthetic Trolox 67.4%) and 10 U/mL of catalase (65.8%). Although lowering the dose of NPs will lead to an expected reduced elimination, 10 μg/mL of NPs presented the H_2O_2 detoxifying ability comparable to the natural enzyme. Additionally, the multifunctional ROS probe CellROX® Orange can also be oxidized by ·OH, the product of H_2O_2, catalysed by transition metal compounds. The significant decrease of the fluorescent intensity in the NPs-added groups thus suggest that the H_2O_2 scavenging activity of FeCo-PBA NPs does not depend on the generation of OH radicals, which is consistent with the previous research using PB NPs.[26] The elimination of 58.3 and 80.3% of $\cdot O_2^-$ radicals can be witnessed when 10 and 20 μg/mL of FeCo-PBA NPs is used as scavengers, respectively. The figures are both lower than those obtained by using 2 U/mL of the natural $\cdot O_2^-$ antidotal enzyme SOD (more than 90%), but either comparable or significantly higher than that for 1 mM of Tempol (~60%). Our results thus suggest that FeCo-PBA NPs also possess SOD-like activity and that this activity is dose-dependent. Hence, effective elimination of SOD can be achieved by optimizing the dosage of SOD according to specific requirements in applications.

It has been reported that H_2O_2 can be oxidized or reduced through two electron transfer channels in PB, high-spin $Fe^{3+/2+}$ and low-spin $Fe(CN)_6^{3-/4-}$, respectively (via Reactions (1) and (2)).[23] When the electrode potential is lower than 0.7 V, the electron transfer of high-spin $Fe^{3+/2+}$ plays the main role, whereas low-spin $Fe(CN)_6^{3-/4-}$ is predominant when the

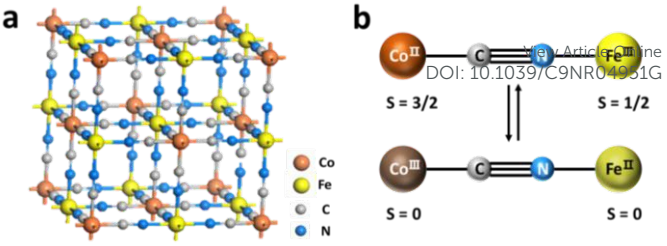

Fig. 2 Schematic representation of a Fe/Co Prussian blue network and its interconversions. (a) The structure of FeCo-PBA with composition $Co_3(Fe(CN)_6)_2$. (b) Interconversion between the paramagnetic (Fe^{III}_{LS}–CN–Co^{II}_{HS}) and diamagnetic (Fe^{II}_{LS}–CN–Co^{III}_{LS}) electronic configuration due to the ROS induced metal-to-metal electron transfer processes.

Table 1. Catalase mimicking activity of FeCo-PBA NPs.

Treatment	H_2O_2 elimination (%)		Treatment	$\cdot O_2^-$ elimination (%)	
	Pristine [a]	80 °C [a]		Pristine [a]	80 °C [a]
H_2O_2 [b]	0.0	0.0	X + XO [b]	0.0	0.0
H_2O_2 + Trolox	67.4±2.5	34.2±2.7	X + XO + Tempol	60.1±4.6	40.3±3.5
H_2O_2 + Catalase	65.8±1.7	20.5±3.4	X + XO + SOD	90.2±2.8	6.2±5.2
H_2O_2 + 10 μg/mL FeCo-PBA NPs	59.5±3.2	57.3±2.2	X + XO + 10 μg/mL FeCo-PBA NPs	58.3±2.9	60.1±1.9
H_2O_2 + 20 μg/mL FeCo-PBA NPs	79.9±1.1	80.8±1.9	X + XO + 20 μg/mL FeCo-PBA NPs	80.3±2.2	80.2±3.0

[a] Pristine for scavengers used directly; 80 °C referring to the pretreatment temperature.
[b] The elimination of the groups without any ROS-scavengers was defined as 0.0% for comparison.

View Article Online
DOI: 10.1039/C9NR04951G

electrode potential reaches 0.9 V. In addition, with these cyanide-bridged bimetallic tridimensional coordination networks, PBNPs can also efficiently quench $\cdot O_2^-$, displaying SOD-like activity (Reaction (3)).[23] As shown in the framework structure of the ideal cubic PBA (Fig. 2(a)), its composition is $CoFe(CN)_6$, in which the (Fe + Co)/CN molar ratio is 1/3. Due to a reversible metal-to-metal electron transfer process between the cobalt and iron centers, switching between paramagnetic ($Fe^{III}{}_{LS}$–CN–$Co^{II}{}_{HS}$) and diamagnetic ($Fe^{II}{}_{LS}$–CN–$Co^{III}{}_{LS}$) configurations (Fig. 2(b); with LS: low Spin and HS: high Spin), PBA NPs can also display ROS scavenging abilities for controlling ROS-induced cell damage.

$$H_2O_2 \rightarrow O_2 + 2e^- + 2H^+ \quad (1)$$

$$H_2O_2 + 2e^- + 2H^+ \rightarrow 2H_2O \quad (2)$$

$$2 \bullet OOH \xrightarrow{SOD/PBNPs} H_2O_2 + O_2 \quad (3)$$

In order to test the thermal stability of FeCo-PBA NPs induced ROS detoxifying ability (especially when they are subjected to a higher temperature), which may determine their potential applications, all the ROS scavengers (in solutions) used in this study (FeCo-PBA NPs, synthetic Trolox/Tempol, and natural enzymes) are pre-treated at 80 °C for 1 h, before their H_2O_2 and $\cdot O_2^-$ elimination efficiencies were tested. As detailed in Table 1, the natural enzymes, the functions of which are usually temperature-dependent, have lost most of their ROS scavenging activities, especially in the case of SOD. The abilities of the Trolox and Tempol both can be preserved by around 50% after thermal pre-treatment. And yet, it is encouraging to see that the FeCo-PBA NPs show significantly better thermal stability with almost all the elimination efficacy retained. Similar results were also reported in researches using Mn based nanoparticles,[35] further highlighting the feasibility of the nano-enzymes operation at higher temperatures.

Cell viability and growth of *S. cerevisiae* cells with FeCo-PBA NPs

To investigate the possible toxicity of the synthesized FeCo-PBA nanoparticles against cells (*S. cerevisiae*), we firstly perform the staining assay on this yeast under the treatment of FeCo-PBA NPs at different concentrations. The results show that these nanoparticles have no obvious inhibition effects on *S. cerevisiae* cells (Fig. 3(a) and Fig. S4, ESI†), and that uptake of NPs does not lead to an increase of intracellular ROS (Fig. S5, ESI†, tested using CellROX® Orange ROS kit after cells co-cultured with NPs for 1h). In other words, the FeCo-PBA nanoparticles are biocompatible and with low toxicity to yeast cells even when the dosage is up to 100 μg/mL. Cell growth of *S. cerevisiae* in YPD media containing FeCo-PBA at different concentrations is then monitored inside a micro-plate reader for 24 h period (Fig. S6, ESI†). The results show that the addition of FeCo-PBA enhances the proliferation of yeast cells. The enhancement is dose-dependent. Indeed, 5 μg/mL of FeCo-PBA increases the cell proliferation by 3.5% while 100 μg/mL by 10.8% compared to the control.

Cell growth is accompanied with metabolic processes and the generation of ROS. The existence of exotic ROS scavengers

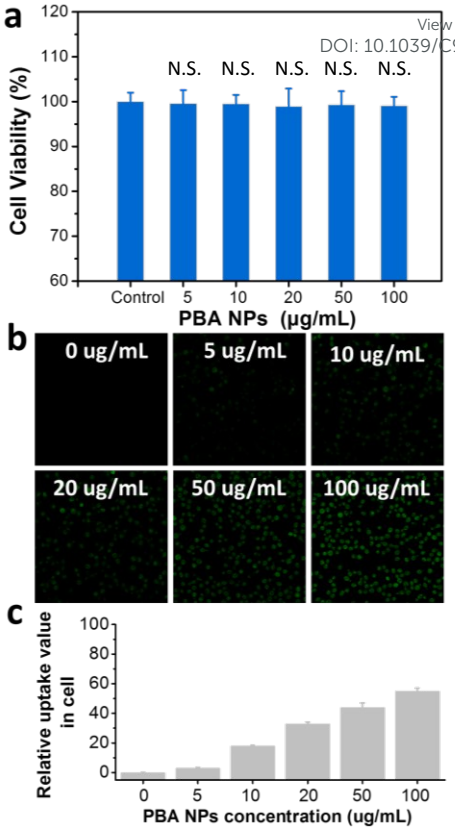

Fig. 3 (a) Cell viability of *S. cerevisiae* under different concentrations of PBA NPs. (b) and (C) Cellular uptake of *S. cerevisiae* under different concentrations of PBA NPs. *S. cerevisiae* cells were incubated in YPD medium containing PBA NPs with the indicated concentrations (5-100 μg/mL). Cell viability was assessed via MB staining method. NPs uptake level was expressed by relative fluorescence intensity. The data points and error bars represent the averages and standard deviations from three independent measurements, respectively.

would then inhibit the accumulation of those ROS and the emergence of oxidative stress in cells. These results indicate that FeCo-PBA can play positive roles during cell growth, indicating their potential for applications as promoters of targeted products in bio-engineering and drug delivery vectors in bio-medicine. Higher concentrations of nanoparticles (within appropriate ranges) in the culture solutions are easier for cellular uptake effectively modifying metabolic activity of the cells.[36] The cellular uptake of FeCo-PBA NPs in *S. cerevisiae* cells is then studied by the inverted confocal laser microscope (Olympus FV3000) with the excitation wavelength at 512 nm and the fluorescence emission maximum at 600 nm. FeCo-PBA NPs emit green fluorescence, which makes them easy to detect inside the cells. From the confocal images (Fig. 3(b)), it is confirmed that the FeCo-PBA NPs can enter the cells. Moreover, the cellular uptake of the nanoparticles is improved in a dose-dependent manner as seen in Fig. 3(c), suggesting that the fluorescence intensity is proportional to the NP concentration.

Plasma as a cellular ROS stressor and for enhancing cellular uptake of FeCo-PBA NPs

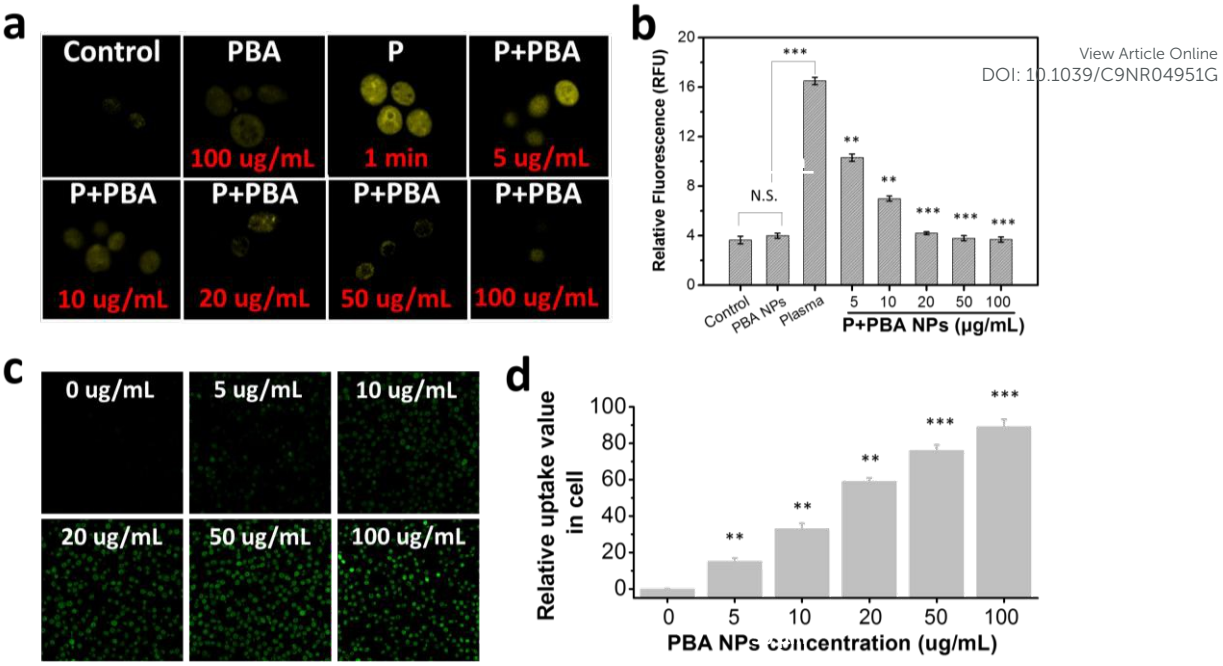

Fig. 4 (a) Fluorescence microscopic images of yeast cells incubated in different concentrated PBA NPs suspensions with and without plasma stress. (b) Intracellular ROS levels in yeast cells incubated in different concentrated PBA NPs suspensions with and without plasma stress. ROS intensity was expressed by relative fluorescence intensity. (c) Cellular uptake of plasma-stressed *S. cerevisiae* under different concentrations of PBA NPs. (d) NPs uptake level was expressed by relative fluorescence intensity. The data points and error bars represent the averages and standard deviations from three independent measurements, respectively.

In order to further validate the ROS scavenging ability of the PBA NPs in cells, APCP is employed to pre-treat the yeast cells. APCP is a multi-modal stressor rich in highly reactive species, UV light and mild heat, well known for its biological activity suitable for sterilization, disinfection and other biomedical applications.[37-40] Longer cell processing times are expected to produce more plasma-related effects, leading to higher cell death rates (Fig. S7, ESI†). Specially, with the plasma exposure for 1 min, the cell viability of *S. cerevisiae* decreases to 91.2% and further falls down to 58.5% when the plasma exposure extends to 10 min. More details about the effects of APCP on the cell viability and growth of *S. cerevisiae* can be found in our previous studies.[41] Since the main purpose of the plasma treatment here is to act as a multifunctional stressor for ROS generation inside the cells, the treatment time is chosen to be 1 min. Under such conditions, a certain amount of reactive species can be delivered to the cells, without any significant cell death effects (i.e., retaining cell viability > 90%). As is seen in Fig. 4(a) and 4(b), 1 min of the APCP treatment significantly increases the intracellular ROS levels in 4 times (from <4 to >16 RFU). Afterwards, the increase in the ROS levels would then be much retarded and the ROS might have even been totally eliminated if the treated cells were cultivated in FeCo-PBA containing broths (containing FeCo-PBA above 20 μg/mL) for a short time (1 h), directly confirming the cellular ROS scavenging ability of the PBA NPs.

It has been previously confirmed that the plasma treatment can modify the cell membranes especially their structure and permeability.[31,42] As indicated in the SEM images (Fig. S8,

Table 2. Ethanol concentration after 24 h of yeast anaerobic fermentation with different amount of FeCo-PBA. Control group corresponds to yeast cells not treated with plasma. Mean values (± SE) for the respective triplicates are given.

FeCo-PBA NPs (μg/mL)	Control Group		1 min Plasma Pretreatment		
	Ethanol (g/L)	L-Increment [a] (%)	Ethanol (g/L)	L-Increment [a] (%)	C-Increment [b] (%)
0	14.93±1.61	--	18.04±1.53	--	20.83
5	16.48±0.73	10.38	22.67±2.14	25.49	37.56
10	18.82±1.04	26.05	28.55±2.59	58.26	51.70
20	22.18±1.34	48.56	33.42±0.81	85.25	50.68
50	25.24±2.56	69.06	36.84±2.59	104.21	45.96
100	27.45±2.64	83.86	37.96±1.31	110.42	38.29

[a] The comparison to the yields obtained without adding FeCo-PBA (longitudinal comparison).
[b] The comparison to the control group with the same amount of FeCo-PBA added (crosswise comparison).

ESI†), the plasma untreated *S. cerevisiae* cells are rounded, with a spherical shape. After the APCP exposure for 1 min, the cell morphology changes to a rough surface. Indeed, a suitable dose of the plasma exposure with a weak electro-magnetic field can enlarge the pores on the surface thus enhancing cell permeability. With longer plasma exposure times, cell surface roughness gradually increased. After 10 min exposure, the cell structure is significantly altered with the cells appearing significantly damaged.

The observed changes in the cell membranes are correlated with the significant boost of the cellular uptake of the FeCo-PBA particles (Fig. 4(c) and 4(d)). Compared to the uptake without the plasma pre-treatment (Fig. 3), considerably more particles can pass through the cell membrane. This effect is confirmed by the higher green fluorescence intensity in the cells when the same dose of the PBA is applied. For example, the NPs uptake value of plasma-treated yeast cells with 20 μg/mL of FeCo-PBA is comparable to that of the untreated cells with 100 μg/mL of FeCo-PBA. This result thus indicates that a moderate APCP treatment might be able to serve as a simple but useful tool to enhance the intracellular utilization efficacy of nanoparticles, while reducing the NP doses. It is also clearly observed from the confocal z-tacking results (Fig. S9, ESI†) that the plasma could enhance the NP cellular uptake but also induce the intercellular oxidative stress. Moreover, the higher concentration of nanoparticles is, the more nanoparticles the cell could uptake. At the same time, the more nanoparticle the cell uptake, the less ROS level is, which indicates the nanoparticle play a role as a ROS-scavenger.

Ethanol production efficiency of *S. cerevisiae* cells with FeCo-PBA NPs

During alcoholic fermentations, yeast cells are subjected to nutritional and environmental stress factors that may trigger the production of large amounts of ROS, affecting DNA, proteins, lipids, the cytoskeleton, and eventually cell survival.[27] Previous studies of ethanol toxicity have found that fermentation product-ethanol may also produce ROS (hydrogen peroxide and superoxide) via generation of hydroxyethyl radical, accumulated at the mitochondrial level and causing cellular damage.[27]

The ethanol yield of *S. cerevisiae* yeast cells after 24 h of the fermentation (glucose concentration: 120 g/L) with different amount of FeCo-PBA NPs (0, 5, 10, 20, 50 and 100 μg/mL) is shown in Table 2. Importantly, the addition of FeCo-PBA NPs boosts the yield of ethanol. The lowest yield (14.93 g/L) is witnessed in the control group, where no FeCo-PBA NPs are added, and then the yields increase with higher concentration of the FeCo-PBA NPs in the culture broth. For example, 10 μg/mL of FeCo-PBA can increase the ethanol production by 26%, and an ethanol concentration of 27.45 g/L (increased by more than 80%) is achieved when the dose of the FeCo-PBA NPs is raised up to 100 μg/mL.

The plasma-exposed cells are transferred into culture broths containing different doses of FeCo-PBA for ethanol production. Consistent with the previous reports, APCP itself can enhance the fermentation efficacy of yeast cells (by around 20%) in anaerobic environment. Indeed, moderate plasma agitation may induce favourable phenotypic or even genotypic changes in the cells. These changes impart the cells with higher tolerance to stress generated during the fermentation, quicker uptake of nutrients (such as glucose), and higher activity of enzymes involved in the metabolic pathways.[32,43]

The PBA presence in the broth significantly increased ethanol production. To be specific, 5 μg/mL of FeCo-PBA leads to the ethanol concentration increased to 22.67 g/L (increased by ~25.5%, compared to the value obtained in PBA free condition), and the production is doubled (to 36.84 g/L) when 50 μg/mL of PBA is applied. In the control group (without the plasma treatment), the highest ethanol production increment (by 83.86%) is obtained with 100 μg/mL of PBA used. Importantly, in the plasma-treated group, only 20 μg/mL is enough to achieve a comparative increment (85.25%). This result indicates that the plasma treatment can significantly reduce the nanoparticle doses to achieve the same or even better results by boosting the NP cellular uptake, which is discussed later. The synergistic effects between the plasma and FeCo-PBA nanoparticles are also confirmed by the C-increment (derived from the comparison of plasma group to the control group with the same amount of FeCo-PBA added), which is always larger than 20.83%.

Upon the plasma treatment, some changes in the call membrane transport may arise due to the direct effect of the plasma (e.g., electrons, ions, chemical reactive species, UV light, moderate heat).[44] By altering the physico-chemical properties of the cell wall and membrane, the cells may attempt

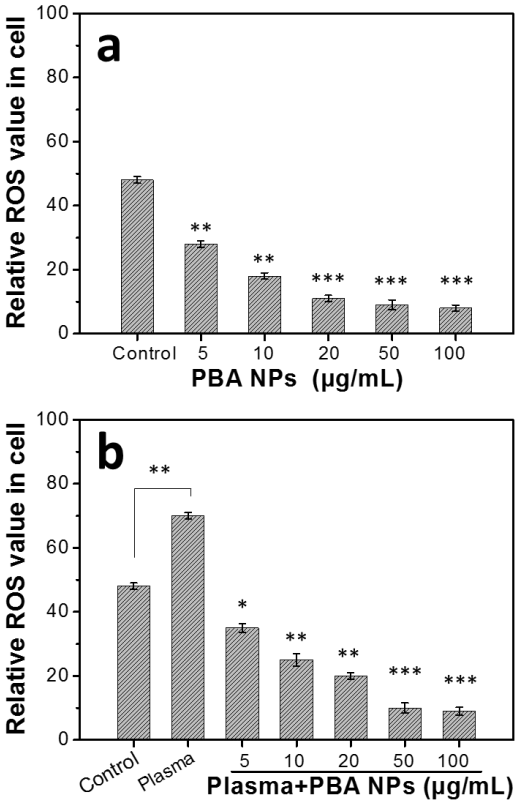

Fig. 5 Intracellular ROS levels in untreated (a) and plasma-treated (b) yeast cells incubated in different concentrated PBA NPs suspensions after fermentation. *S. cerevisiae* cells were cultured in YPD medium containing PBA NPs with the indicated concentrations (5-100 μg/mL). Cells were stained with CellROX® Orange Reagent for 30 mins and observed by fluorescence microscopy (excitation wavelength: 545 nm, emission wavelength: 565 nm). ROS intensity was expressed by relative fluorescence intensity. The data points and error bars represent the averages and standard deviations from three independent experiments, respectively.

to regulate cross-membrane transport and thus prevent damage or withstand external forces from the stressor. Previous studies of CAP-cell interactions have reported pore formation in the cell membrane in response to CAP-generated chemically active species.[31,41,45] These species can induce chemical and physical changes on biological surfaces, however these changes in membrane permeability are generally transient.

Fig. 5 shows the oxidative stress response of the untreated and plasma-treated yeast cells fermented with different concentrations of FeCo-PBA NPs after the fermentation. Compared with the ROS level before the fermentation (Fig. S5, ESI†), which displays a dose-independent behaviour in ROS levels, a significant increase in fluorescence corresponding to intracellular ROS concentration is observed after the fermentation. This may be attributed to the fact that fermentation-generated stress environment contributes to a noticeable rise in intracellular oxidative stress. On the other hand, the addition of PBA NPs at 0–100 μg/mL can effectively inhibit the intracellular ROS generation during the fermentation, due to the cellular uptake of these nanozymes, acting as an intracellular ROS scavenger. All these results are consistent with that of cell viability and proliferation, indicating that PBA NPs may play a protective role against oxidative stress generated from alcoholic fermentation.

Experimental

Synthesis and characterization of FeCo-PBA nanoparticles

In a typical procedure, $Fe(NO_3)_2{\cdot}6H_2O$ (1.73 g, 6.0 mmol) and $K_3Co(CN)_6$ (1.33 g, 4.0 mmol) are dissolved into 200 mL deionized water respectively. Then the above two precursor solutions are mixed under magnetic stirring. The precipitates are collected by centrifugation, washed several times with distilled water and ethanol, and dried at 60 °C in a vacuum oven overnight. The crystalline phases of FeCo-PBA nanoparticles are characterized by X-ray powder diffraction (XRD, PANalytical X'Pert3) equipped with Cu Kα radiation. Scanning electron microscopy (SEM, Tescan MIRA3) and high-resolution transmission electron microscopy (HRTEM, JEOL-2100, 200 kV) are employed to explore the size and morphology of as-prepared samples. X-ray photoelectron spectroscopy (XPS, Kratos Axis) is used to identify the chemical composition and valence state of each element of the materials. Vibrational fingerprints of the chemical bonding of the nanoparticles is identified by Fourier transform infrared spectroscopy (FTIR, Nicoletis 50, ThermoFisher). Ultraviolet-visible (UV-VIS) absorption spectra are recorded on an UV-VIS-NIR spectrophotometer (UV-3600, Shimadzu, Japan).

Extracellular ROS scavenging activities of FeCo-PBA NPs

Catalase mimicking activity measurements. The elimination of H_2O_2 is investigated by measuring the fluorescent intensity. Phosphate buffered saline (PBS, 25 mM, pH 7.4) containing H_2O_2 (10 mM) and FeCo-PBA NPs (with the concentration of 0, 10 or 20 μg/mL) or anti-H_2O_2 reagents (10 U/mL of the natural catalase or 100 μM of synthetic Trolox) are well mixed and then incubated at 37 °C for 6 h. CellROX® Orange (5 μM, Life Technologies, Carlsbad, USA) is then added and another 30 min incubation is undertaken at room temperature, before the fluorescence of the mixture is measured. The elimination percentage for quantitation of the effect of ROS scavenging is calculated using the following equation: elimination (%) = $[(F_0 - F)/F_0] \times 100$, where F_0 is the fluorescence intensity of the group incubated either at room temperature or at 80 °C without any FeCo-PBA NPs and anti-ROS reagents added (termed H_2O_2 only), while F represents the intensities of groups with scavengers. The experiments are done in three independent trials with results shown as the average ± the standard deviation.

SOD mimicking activity measurements. $\cdot O_2^-$ is generated and detected according to former literature.[35] Briefly, xanthine (X, 0.6 mM) and xanthine oxidase (XO, 0.05 U/mL) in phosphate buffer (0.1 M, pH 7.4) are incubated for 40 min at 37 °C for $\cdot O_2^-$ containing solutions preparation, and $\cdot O_2^-$ is then characterized by its specific fluorescence probe hydroethidine (0.5 mg/mL), which can be oxidized by $\cdot O_2^-$ into ethidium with excitation and emission wavelengths at 470 and 610 nm, respectively. For $\cdot O_2^-$ scavenging, 10 or 20 μg/mL of FeCo-PBA NPs, or anti-$\cdot O_2^-$ reagents (2 U/mL of the natural superoxide dismutase (SOD) or 1 mM of the synthetic agent Tempol) is added and incubated at 37 °C for 6 h. The amount of $\cdot O_2^-$ scavenged is then detected again by measuring the fluorescent intensity. And the calculation of $\cdot O_2^-$ elimination is the same as that of H_2O_2.

Thermal stability tests. FeCo-PBA and the anti-ROS reagents (natural enzymes, catalase and SOD, and Trolox/Tempol) are pre-treated for 1 h at 80 °C respectively, before being used to scavenge H_2O_2 and $\cdot O^{2-}$ to compare their thermal stability of ROS scavenging.

Yeast strains and plasma treatment

S. cerevisiae AWRI 1631 is a haploid strain, provided by the Australian Wine Research Institute. It is routinely maintained in a basic YPD agar/medium, which consists of the following ($g{\cdot}L^{-1}$): yeast exacts 10, bacteriological peptone 20, glucose 20, with/without agar 15. *S. cerevisiae* cells are cultured on agar plates at 37 °C and left to grow for 72 h before APCP treatment.[32] Individual colonies with similar size are then subjected to direct APCP exposure for different durations (Fig. S2, ESI†). Plasma is generated using an atmospheric pressure plasma jet (kINPen08, 1.7 MHz, 2-6 kV), and argon (Ar) is used as the feed gas at a flow of 5 standard litre per minute (SLM). The distance between the jet nozzle and yeast colonies is constant (~ 7 mm). More details about the description of this type of plasma jet and biological sample treatment can be found in our previous studies.[32] For the control group, only 5 SLM of Ar gas is fed (without voltage added) and used for the same treatment time for comparison.

Incubation of yeast cells and fermentation with PBA NPs

Fresh YPD medium is used to prepare Fe-Co PBA NPs containing solution with the concentration of 2000 μg/mL.

After being sonicated for 30 min (AS3120, Autoscience, China), the stock solution is ready for being applied in yeast incubation and fermentation. Prior to cell viability tests, the treated or control colonies are transferred into YPD media and seeded at a density of 5000 cells/well in 96-well plates, incubated with or without PBA NPs of different concentration for 1 h. Cell viability was assessed by staining of cells with methylene blue (0.1 mg/mL stock solution, dissolved in a 2% dehydrate sodium citrate solution).[32] Cell growth assay is performed using a Microplate Reader (Bio-Rad 680, USA) at the absorbance of 600 nm for 24 h period.

To test the yeast fermentation efficacy with or without FeCo-PBA, a modified YPD medium (containing 120 g/L of glucose, which is the only difference to pristine YPD) is employed, and PBA in the stock solution is added to the required concentrations. Culture media (30 mL) are then incubated under anaerobic isothermal conditions and at 30 °C for 2 days. More details about the experimental procedure is shown in Fig. S1, ESI†. All fermentation experiments are performed in triplicate.

Ethanol determination. Ethanol production is analyzed with the Ethanol assay kit (Megazyme, Ireland) according to the manufacturer's protocol. 100 μL sample solution, which is diluted 1000 times, mixed with 200 uL distilled water, 20 μL Solution 1 (buffer), 20 μL Solution 2 (Nicotinamide-adenine dinucleotide, NAD^+) and 5 μL Solution 3 (Aldehyde dehydrogenase, AIDH), is placed at room temperature with the reaction time of 5 min and measured with a microplate reader at a wavelength of 340 nm. The reactions are then started by addition of 2 μL Suspension 4 (Alcohol dehydrogenase, ADH) and the absorbances are continuously read at 1 min intervals until the absorbances increase constantly over 1 min. Absorbance values are calibrated by a single point standard solution diluted properly when highly concentrated using the same batch of regents. The calculation (Microplate Assay Procedure):

$$\text{Ethanol yield (g/L)} = \frac{\Delta A_{\text{sample}}}{\Delta A_{\text{standard}}} \times \text{standard concentration} \times \text{F}$$

where F is the dilution factor of the sample solution.

Intracellular ROS detection. Intracellular ROS generation is again determined by CellROX® Orange Reagent according to the manufacturer's instructions. CellROX® Orange Reagent is an ideal fluorogenic probe for measuring oxidative stress in live cells.[32] This cell-permeant dye is non-fluorescent while in a reduced state exhibits bright fluorescence upon oxidation by ROS. Cells are analysed with the Promega GloMax plate reader at an excitation and emission wavelength of 545 and 565 nm respectively.

Statistical analysis. Results are expressed as the mean ± SD (range) or a percentage value. Comparisons between groups were made using Student's unpaired t-test. Statistical significance of P-values was represented. $*p < 0.05$, $**p < 0.01$, $***p < 0.001$, $****p < 0.0001$. All calculations were performed using the GraphPad Prism software package (GraphPad Software Inc., San Diego, CA, USA).

Conclusion

View Article Online
DOI: 10.1039/C9NR04951G

In summary, we synthesize Prussian Blue Analogue (PBA) nanoparticles (nanoenzymes) with good biocompatibility and ROS scavenging ability. The PBA nanoenzymes are successfully used in conversion of glucose to ethanol during yeast fermentation, the efficacy of which depends mainly on the yeast's ability to counteract the stress factors during the process. Our results show that the PBA NPs can protect cells from oxidative stress induced by both the plasma exposure and fermentation processes. As a result, the secondary metabolite yields and energy production are improved. This work confirms the positive effects of PB-based NPs in living cells and their ROS scavenging ability, vitally needed for the development of next-generation nanotechnology-enabled oxidative stress mediators for diverse applications in biotechnology and biomedicine.

Conflicts of interest

The authors declare no competing financial interest.

Acknowledgements

This work was partially supported by the Australian Research Council (ARC). The Translational Research Institute (TRI) receives funding from the Australian Government. We acknowledge supports from the Central Analytical Research Facility operated by the Institute of Future Environment (QUT). The authors would also like to thank Mr. Rusen Zhou for his kind assistance in manuscript revision.

Notes and references

1 B. Yang, Y. Chen and J. Shi, *Chem. Rev.*, 2019, **119**, 4881-4985.
2 B. D'Autréaux and M. B. Toledano, *Nat. Rev. Mol. Cell Bio.*, 2007, **8**, 813.
3 B. C. Dickinson and C. J. Chang, *Nat. Chem. Bio.*, 2011, **7**, 504.
4 C. Nathan and A. Cunningham-Bussel, *Nat. Rev. Immunol.*, 2013, **13**, 349.
5 H. Guo, J. B. Callaway and J. P. Ting, *Nat. Med.*, 2015, **21**, 677.
6 Q. Cui, J. Wang, Y. G. Assaraf, L. Ren, P. Gupta, L. Wei, C. R. Ashby Jr, D. Yang and Z. Chen, *Drug Resist. Update.*, 2018, **41**, 1-25.
7 H. Jia, D. Yang, X. Han, J. Cai, H. Liu and W. He, *Nanoscale*, 2016, **8**, 5938-5945.
8 X. Wang, X. J. Gao, L. Qin, C. Wang, L. Song, Y. Zhou, G. Zhu, W. Cao, S. Lin and L. Zhou, *Nat. Commun.*, 2019, **10**, 704.
9 S. Nakajima, I. Ohsawa, K. Nagata, S. Ohta, M. Ohno, T. Ijichi and T. Mikami, *Behav. Brain Res.*, 2009, **200**, 15-21.
10 J. M. Matés, C. Pérez-Gómez and I. N. De Castro, *Clin. Biochem.*, 1999, **32**, 595-603.
11 R. Breslow, *Accounts Chem. Res.*, 1995, **28**, 146-153.
12 P. V. Iyer and L. Ananthanarayan, *Process Biochem.*, 2008, **43**, 1019-1032.
13 S. R. Doctrow, K. Huffman, C. B. Marcus, W. Musleh, A. Bruce, M. Baudry and B. Malfroy, *Advances in Pharmacology*, Elsevier, 1996, **38**, 247-269.
14 B. J. Day, *Biochem. Pharmacol.*, 2009, **77**, 285-296.
15 C. Ge, G. Fang, X. Shen, Y. Chong, W. G. Wamer, X. Gao, Z. Chai, C. Chen and J.-J. Yin, *ACS Nano*, 2016, **10**, 10436-10445.

View Article Online
DOI: 10.1039/C9NR04951G

16 H. Wei and E. Wang, *Chem. Soc. Rev.*, 2013, **42**, 6060-6093.
17 J. Wu, X. Wang, Q. Wang, Z. Lou, S. Li, Y. Zhu, L. Qin and H. Wei, *Chem. Soc. Rev.*, 2019, **48**, 1004-1076.
18 B. Liu and J. Liu, *Nano Res.*, 2017, **10**, 1125-1148.
19 B. Liu and J. Liu, *Nanoscale*, 2015, **7**, 13831-13835.
20 F. Yang, S. Hu, Y. Zhang, X. Cai, Y. Huang, F. Wang, S. Wen, G. Teng and N. Gu, *Adv. Mater.*, 2012, **24**, 5205-5211.
21 L. Jing, X. Liang, Z. Deng, S. Feng, X. Li, M. Huang, C. Li and Z. Dai, *Biomaterials*, 2014, **35**, 5814-5821.
22 L. Su, Y. Xiong, H. Yang, P. Zhang and F. Ye, *J. Mater. Chem. B*, 2016, **4**, 128-134.
23 W. Zhang, S. Hu, J.-J. Yin, W. He, W. Lu, M. Ma, N. Gu and Y. Zhang, *J. Am. Chem. Soc.*, 2016, **138**, 5860-5865.
24 M. Shokouhimehr, E. S. Soehnlen, J. Hao, M. Griswold, C. Flask, X. Fan, J. P. Basilion, S. Basu and S. D. Huang, *J. Mater. Chem.*, 2010, **20**, 5251-5259.
25 D. Aguila, Y. Prado, E. S. Koumousi, C. Mathoniere and R. Clérac, *Chem. Soc. Rev.*, 2016, **45**, 203-224.
26 M. Vázquez-González, R. M. Torrente-Rodríguez, A. Kozell, W.-C. Liao, A. Cecconello, S. Campuzano, J. M. Pingarrón and I. Willner, *Nano Lett.*, 2017, **17**, 4958-4963.
27 R. V. Perez-Gallardo, L. S. Briones, A. L. Díaz-Pérez, S. Gutiérrez, J. S. Rodríguez-Zavala and J. Campos-García, *FEMS Yeast Res.*, 2013, **13**, 804-819.
28 J. Guo, M. Suástegui, K. K. Sakimoto, V. M. Moody, G. Xiao, D. G. Nocera and N. S. Joshi, *Science*, 2018, **362**, 813-816.
29 H. Alper, J. Moxley, E. Nevoigt, G. R. Fink and G. Stephanopoulos, *Science*, 2006, **314**, 1565-1568.
30 C. Willyard, *Nature News*, 2017, **542**, 406.
31 J. Van der Paal, E. C. Neyts, C. C. Verlackt and A. Bogaerts, *Chem. Sci.*, 2016, **7**, 489-498.
32 N. Recek, R. Zhou, R. Zhou, V. S. J. Te'o, R. E. Speight, M. Mozetič, A. Vesel, U. Cvelbar, K. Bazaka and K. K. Ostrikov, *Sci. Rep.*, 2018, **8**, 8252.
33 R. Sharma, M. A. Iqubal, S. Jheeta and Kamaluddin, *Inorganics*, 2017, **5**, 18.
34 F. Zheng, D. Zhu, X. Shi and Q. Chen, *J. Mater. Chem. A*, 2015, **3**, 2815-2824.
35 J. Yao, Y. Cheng, M. Zhou, S. Zhao, S. Lin, X. Wang, J. Wu, S. Li and H. Wei, *Chem. Sci.*, 2018, **9**, 2927-2933.
36 Q. Mu, G. Jiang, L. Chen, H. Zhou, D. Fourches, A. Tropsha and B. Yan, *Chem. Rev.*, 2014, **114**, 7740-7781.
37 R. Zhou, R. Zhou, P. Wang, B. Luan, X. Zhang, Z. Fang, Y. Xian, X. Lu, K. Ostrikov and K. Bazaka, *ACS Appl. Mater. Inter.*, 2019, In press http://doi.org/10.1021/acsami.9b03961.
38 R. Zhou, R. Zhou, F. Yu, D. Xi, P. Wang, J. Li, X. Wang, X. Zhang, K. Bazaka and K. K. Ostrikov, *Chem. Eng. J.*, 2018, **342**, 401-409.
39 R. Zhou, R. Zhou, K. Prasad, Z. Fang, R. Speight, K. Bazaka and K. K. Ostrikov, *Green Chem.*, 2018, **20**, 5276-5284.
40 F. Dong, J. Zhang, K. Wang, Z. Liu, J. Guo and J. Zhang, *Nanoscale*, 2019, **11**, 1123-1130.
41 K. Prasad, N. Recek, R. Zhou, R. Zhou, M. Aramesh, A. Wolff, R. Speight, M. Mozetič, K. Bazaka and K. K. Ostrikov, *Sustainable Materials and Technologies*, 2019, **22**, e00123
42 N. Recek, X. Cheng, M. Keidar, U. Cvelbar, A. Vesel, M. Mozetic and J. Sherman, *PloS One*, 2015, **10**, e0119111.
43 X. Zhang, X. F. Zhang, H. P. Li, L. Y. Wang, C. Zhang, X. H. Xing and C. Y. Bao, *Appl. Microbiol. Biot.*, 2014, **98**, 5387-5396.
44 H. Li, W. Sun and K. Ostrikov, *Phys. Rep.* 2018, **770–772**, 1-45.
45 A. Bogaerts, M. Yusupov, J. Razzokov and J. Paal, *Front. Chem. Sci. Eng.*, 2019, **13**, 253-263.

View Article Online
DOI: 10.1039/C9NR04951G

Journal Name

ARTICLE

Table of contents

Prussian Blue Analogue Nanoenzymes Mitigate Oxidative Stress and Boost Bio-Fermentation

Renwu Zhou, Peiyu Wang, Yanru Guo, Xiaofeng Dai, Shaoqing Xiao, Zhi Fang, Robert Speight, Erik W. Thompson, Patrick J. Cullen and Kostya (Ken) Ostrikov

This work demonstrated the efficacy of Prussian blue analogue nanoparticles (FeCo-PBA NPs) as effective scavenger of reactive oxygen species under plasma-controlled cellular stress conditions and booster of ethanol fuel production by yeast fermentation.